J. Phys.: Condens. Matter 7 (1995) 1755–1769. Printed in the UK

The atomic-scale structure of amorphous hydrogenated carbon

J K Walters and R J Newport
Physics Laboratory, The University, Canterbury, Kent CT2 7NR, UK

Received 16 November 1994

Abstract. The structure of a common batch of amorphous hydrogenated carbon samples (a-C:H) has been studied in detail using time of flight neutron diffraction, inelastic neutron scattering, NMR and molecular dynamics (MD) simulation. Supplementary work has included differential scanning calorimetry (DSC), infrared (IR) spectroscopy and combustion analysis. A summary of the results is presented as evidence for a new structural model for a-C:H.

1. Introduction

The last two decades have seen a continued growth in our knowledge of amorphous materials and our understanding of their properties, together with an increased technological exploitation. Amorphous materials have maintained their position of fundamental as well as technological interest due to the increasing complexity of the materials being produced, so that important questions concerning their properties remain unanswered. A prime example of this is the now extensive work on amorphous hydrogenated silicon, a-Si:H [1]. Indeed, it is almost axiomatic that, as novel materials continue to be generated, the range of questions only increases.

The material at the focus of our investigations here, amorphous hydrogenated carbon, a-C:H, is of particular interest as it may be prepared harder, denser and more resistant to chemical attack than any other solid hydrocarbon [2, 3], which, together with the high degree of transparency to the infrared and histocompatibility, have led to many applications [4, 5].

2. Background

Carbon is probably the most widely studied of the known elements. The electronic structure of carbon ($1s^2\ 2s^2\ 2p^2$) makes this element unique in its ability to form three different types of covalent chemical bond i.e. three different hybrid orbitals: sp^3 (found in diamond), sp^2 (found in graphite) and sp^1 (found in acetylene, C_2H_2). Perhaps the most familiar forms of carbon are diamond and graphite, but other forms do exist [6]. Graphite is the most stable form with a hexagonal layer structure in which each carbon atom is sp^2 bonded and has three nearest-neighbour atoms in a two-dimensional arrangement (σ bonded). The remaining π type orbital lies perpendicular to this plane as a 'dangling bond' or π electron band. On the other hand, cubic diamond is metastable and has a tetrahedral structure with only sp^3 bonding and no 'dangling bonds'.

0953-8984/95/091755+15$19.50

Most authors agree that a-C:H contains a mixture of sp^3, sp^2 and (sometimes) sp^1 carbon bonding. However, the main questions concern the relative amounts of each of these bonding types and their distribution within the structure. The nature of the carbon bonding is determined by the conditions under which the a-C:H was prepared [2] and a mechanism describing the deposition process, the subplantation model, has been developed by Lifshitz and co-workers [7, 6]. For example, a-C:H can be prepared in forms varying from the soft polymeric (high hydrogen content with many $-CH_2-$ chains) at one extreme to graphitic (high sp^2 content, low hydrogen content) at the other. Polymeric a-C:H films are deposited under conditions having intrinsically low incident particle energies, whereas the graphitic analogue arises from deposition conditions in which there are high incident energies which causes preferential sputtering of hydrogen. Hard, or 'diamond-like', a-C:H forms under conditions of intermediate deposition energies, which result in a large degree of cross-linking and structural rigidity and intermediate hydrogen content [2]. It is clear then that the macroscopic properties of a-C:H, and therefore its potential applications, also depend critically on the conditions under which it was prepared.

It is also necessary to consider the role of hydrogen in these materials. There is evidence [8] that hydrogen tends to satisfy any 'dangling bonds', so, primarily, hydrogen incorporation will saturate π bonds thereby converting sp^2 carbon to sp^3 carbon sites. Most studies agree that hydrogen bonds to both sp^2 and sp^3 carbon, but preferentially to sp^3 carbon. For example, infrared data [9, 10, 11] find mainly sp^3 C–H bonds in hard a-C:H, and find sp^3 CH_3, sp^3 CH_2 and sp^2 CH_2 bonds in soft a-C:H. The incorporation of hydrogen is also found to lower the density of the material [8]. This is not primarily an effect of the low mass of the hydrogen atom, but reflects the reduced amount of cross-linking in the carbon network due to the presence of hydrogen. Hydrogen incorporation and/or graphitic bonding both tend to result in a reduction of the average coordination number [2]. There is also evidence to suggest that some of the hydrogen in a-C:H is not chemically bonded to carbon [12], with the possibilities of hydrogen being (a) bound and in clusters [13]; (b) intercalated between turbostatic graphite layers; and (c) chemisorbed on internal surfaces. The presence of hydrogen not bonded to carbon also indicates the presence of microscopic and macroscopic voids throughout the volume of the material.

So, in spite of the great potential of the material and the studies so far undertaken, the structure of these materials at the atomic level is not fully understood.

3. Structural models for a-C:H

The simplest model consistent with H:C and sp^2:sp^3 ratios is a 'Polk' type model [14]. This consists of a covalent random network of tetrahedrally and trigonally coordinated carbon atoms with some bonds terminated by hydrogen [15, 10]. This model gives a simple, homogeneous structure, however experimental data suggest that the structure may be more heterogeneous. In interpreting optical constants, Smith [16] envisaged a multiphase structure of amorphous graphitic, diamond-like and polymeric regions with a heterogeneous distribution of hydrogen over the different carbon fractions. Electron spin resonance (ESR) [17] and electron energy loss spectroscopy (EELS) [18] data have been used to suggest a structure where regions of polycyclic aromatic hydrocarbon are interconnected with sp^3 carbon. However, the model most commonly used in the interpretation of experimental results at present is the non-crystalline 'two-phase' model [18], which originated from electron diffraction data [19]. The first phase consists of π bonded (sp^2) clusters, which are embedded in the second phase, an sp^3 bonded phase, which in hard a-C:H is highly cross-linked, and in soft a-C:H is a polymeric hydrogenated phase. The sp^2 phase determines the

optical properties of the material, while the sp^3 phase determines its mechanical properties. This model was subsequently adopted by Robertson [20] and formed the basis of his quantum chemical calculations which will now be discussed in more detail.

Robertson took the two-phase model and used theoretical calculations to obtain detailed information on the two phases, particularly the extent and structure of the sp^2 phase [20, 21]. One reason for first proposing a model with aromatic clusters embedded in an sp^3 matrix was the relatively small band gap measured for a-C and for many a-C:H samples (~1–2 eV). This cluster model was developed using Huckel calculations to model the electronic density of states measured experimentally. A key feature of this method is that creating a band gap at the Fermi energy, E_F will lower the energy of the occupied states and stabilize the structure.

The Huckel model [20] uses a simplified tight-binding Hamiltonian considering only the π orbitals and nearest-neighbour interactions. In this way sp^3 sites are seen as blocking the π interaction from passing through that site (as there are no π states present at that site). So the Huckel model maps the C–H network onto a series of π bonded clusters and finds a stable structure by maximizing the total binding energy per site (E_{tot}) of each cluster.

Investigations using many possible structures led to the following observations [21]:

(1) Clusters tend to be planar.

(2) There should be an even number of sites in each cluster.

(3) Olefinic chains are not particularly favoured.

(4) E_{tot} is dramatically reduced when aromatic rings form in the structure.

(5) E_{tot} is increased if the aromatic rings are fused into layers $\Rightarrow$ graphitic (layer) clusters are favoured over acenic (row) clusters.

(6) Compact clusters are favoured over acenic clusters.

(7) Quinoid groups are unfavoured.

(8) Fourfold, fivefold, sevenfold and eightfold rings are unfavoured.

Using this information therefore, we can see that the band gap depends mainly on the medium range ordering (MRO), i.e. the degree of clustering. For example, the Huckel model gives the following results, where M is the number of rings:

(i) for hard a-C:H, typical band gap = 1.2 eV: $M = 25$ (largest clusters), $M = 6$ (average cluster)

(ii) for soft a-C:H, typical band gap = 2.5 eV: $M = 5$ (largest clusters), $M = 2$ (average cluster).

The important conclusions from this model are that π bonding strongly favours aromatic rings over olefinic chains and favours the clustering of separate rings into graphitic sheets, making aromatic ring clusters the dominant sp^2 site species. Bredas and Street [22] independently reached the same conclusions using a more sophisticated model.

Note that a necessary part of the Huckel model is that σ and π states can be treated separately. This is justified because the sp^2 clusters tend to be planar so that parallel π states on adjacent sites tend to lie perpendicular to the σ-bonding plane. However, any warping or cross-connection of sp^2 layers may produce σ–π mixing.

This model reproduces the experimentally observed density of states quite well and has made a valuable contribution to the recent progress in this field of study. However, there are some questions which should be raised at this point. Aromatic ring clusters model the data well, but is it *possible* to model the data using an arrangement of olefinic sp^2 sites? Looking at the evidence from molecular dynamics simulations [23, 24] the answer to this question is positive and this will be discussed later. Also the Huckel model uses only the π

orbitals and their nearest-neighbour interaction. This appears to be an oversimplification of the real situation especially as the π bonding in carbon ring structures will be delocalized so that their bonding energy is longer ranged and therefore non-local.

Experimental data cited in support of this model comes mainly from optical spectra [25], Raman spectroscopy [26] and luminescence spectroscopy [27, 28]. However, although each of these provide clear evidence for the presence of an sp^2 phase, there is no conclusive evidence for graphitic clustering.

Our recent work, brought together here, will show that this model for a-C:H is inadequate, and indeed no evidence for any graphitic sp^2 phase in a-C:H is found.

4. Experimental results

The preparation and properties of the samples used in this study are summarized in table 1 and more details can be found in [29, 30].

Table 1. Information on the samples studied. (FAB ≡ fast-atom (neutral particle) beam source; PECVD ≡ plasma enhanced chemical vapour deposition). Note that for the sample prepared by PECVD the energy is the mean ion energy, whereas for the FAB samples it it the effective source energy.

Sample	Precursor gas	Preparation method	Energy (eV)	H (at.%)	Density (g cm^{-3})
1	acetylene	FAB	~500	35	1.8
2	propane	FAB	~500	32	2.0
3	acetylene	PECVD	~30	44	1.4

4.1. Neutron diffraction

The data were collected using the LAD diffractometer at the ISIS pulsed neutron facility at the Rutherford Appleton Laboratory (UK) [31]. The wide dynamic range available on this instrument (~ 0.2–50 Å^{-1}) allows high-resolution real space data to be obtained. This is a significant improvement on the quality of information gained from other diffraction techniques which are unable to distinguish different carbon bonding environments and do not detect hydrogen well. Full experimental details are given in [29] and [32]. The experimental data undergo several corrections before a structure factor, $S(Q)$, directly related to the scattered neutron intensity, is obtained [33]. By Fourier transformation, real space information is obtained in the form of a pair correlation function, g(r), using the equation

$$S(Q) = 1 + \frac{4\pi\rho}{Q}\int_0^\infty r\,dr(g(r) - 1)\sin(Qr) \tag{1}$$

where ρ is the average number density of atoms in the material, $|Q| = |k_i - k_f|$ is the wavevector transfer associated with the diffraction experiment—for elastic scattering from a liquid or amorphous solid, $Q = (4\pi/\lambda)\sin\theta$, where 2θ is the scattering angle and λ is the neutron wavelength. For a binary system such as a-C:H, there are contributions to the structure factor from each atom type pair, i.e. there are three independent contributions, which are weighted to give the total structure factor. The corresponding real space function,

the total pair correlation function, $G(r)$, is a weighted combination of the partial pair distribution functions, and is defined (according to the Faber–Ziman formalism [34]) as:

$$G(r) = \sum_{\alpha,\beta} \left[c_\alpha c_\beta b_\alpha b_\beta g_{\alpha\beta}(r) \right] \tag{2}$$

where c_α is the atomic fraction and b_α the coherent scattering length respectively of element α; and where $g_{\alpha\beta}(r)$ represent the partial terms in $G(r)$ and describe the probability of finding an atom of type β at a distance r from an atom of type α at the origin. The weightings of the partial terms mean that the dominant terms are those arising from carbon–carbon correlations and carbon–hydrogen correlations, with the carbon–hydrogen correlations appearing as troughs rather than peaks, since b_H is negative (due to the π phase shift experienced by a neutron on scattering from hydrogen. It must also be equivalent to the hydrogen–carbon term). These equations rely on the static approximation [35, 36] being valid, i.e. that the change in the neutron's energy on scattering is small compared to its incident energy. $G(r)$ can be converted to a radial distribution function, $J(r) = 4\pi r^2 \rho G(r)$ and then fitted with a series of Gaussians, allowing position and area to vary. By this method accurate values for the bond lengths and coordination numbers can be obtained.

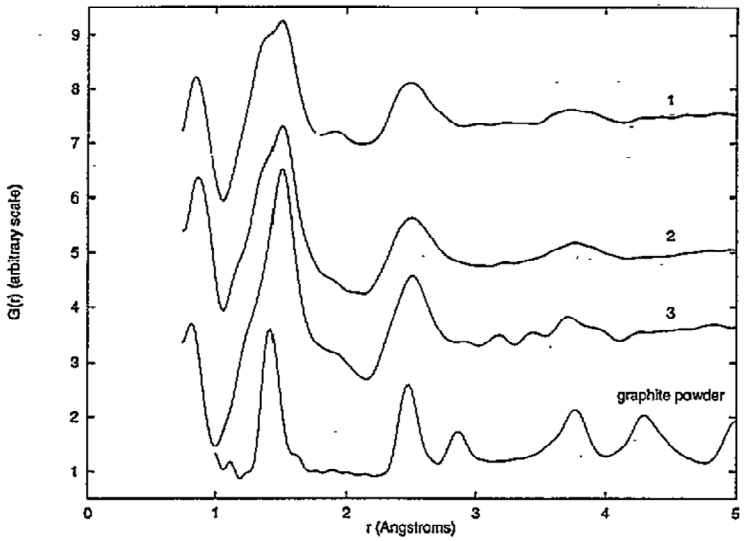

Figure 1. Pair correlation functions for samples 1, 2, 3 and graphite powder (offset) obtained from neutron diffraction experiments on the instrument LAD [29, 32].

Figure 1 shows the pair correlation functions obtained for the three different samples (deposited using two different techniques) and graphite powder, for comparison, with the results of the Gaussian fitting given in tables 2, 3 and 4, respectively. Immediately it is clear that with such high real space resolution all three hybridization states of carbon are observed: sp^3 C–C at ~1.53 Å, sp^2 C=C at ~1.34 Å and sp^1 C≡C at 1.18 Å. Also peaks at ~0.86 Å give clear evidence for the presence of molecular hydrogen in these samples in relatively small quantities. The C–C bond lengths are slightly less than those associated with saturated C–C in diamond, which is consistent with the proximity of sp^2 carbon atoms to the single bond. In samples 1, 2 and 3, an unsaturated C=C bond length of 1.34 Å is observed which, because of its exact correspondence with the bond length associated with olefinic sp^2 C=C bonds, indicates that most of the sp^2 carbon present is of the olefinic, not

the aromatic/graphitic form [29]. This can also be seen by comparison with the data shown for graphite which have a single peak at 1.42 Å. For samples 1 and 2, the sp^3:sp^2 bond ratio is found to be ~2.5:1 (but could be as high as 3.7:1 within the experimental errors in $J(r)$) and for sample 3 the ratio sp^1:sp^2:sp^3 is 0.13:0.14:1.

Table 2. *Bond lengths and coordination numbers for sample 1 derived from the neutron data.*

Peak position (± 0.01 Å)	Peak area (± 0.3 atoms)	Assignment
0.88	0.84	H–H
1.03	0.18	C–H and H–C
1.34	0.84	C=C
1.52	2.17	C–C
1.7–2.2		H–C–H and C–C–H
~ 2.5		C–C–C

Table 3. Bond lengths and coordination numbers for sample 2 derived from the neutron data.

Peak position (± 0.01 Å)	Peak area (± 0.3 atoms)	Assignment
0.86	0.41	H–H
1.06	0.16	C–H and H–C
1.34	1.12	C=C
1.53	2.64	C–C
1.7–2.2		H–C–H and C–C–H
~ 2.5		C–C–C

Table 4. Bond lengths and coordination numbers for sample 3 derived from the neutron data.

Peak position (± 0.01 Å)	Peak area (± 0.3 atoms)	Assignment
0.85	0.18	H–H
1.04	0.78	C–H and H–C
1.18	0.31	C≡C
1.34	0.34	C=C
1.51	2.40	C–C
1.7–2.2		H–C–H and C–C–H
~ 2.5		C–C–C

It is also possible to make assignments beyond the first coordination shells. For each of the samples there is a small peak at ~1.9 Å which is possibly the result of a convolution of the large carbon–carbon second-shell-neighbour peak at ~2.5 Å with a 'negative feature' at 2.16 Å due to an sp^3 C–C–H second-shell correlation; it is more likely however that it arises from an sp^3 or sp^2 H–C–H second-shell correlation (which would be expected at ~1.8–1.9 Å, the precise distance depending on the associated bond angle—i.e. on whether the CH_2 is sp^2 or sp^3 in nature). Indeed, if short chains of sp^3 CH_2 exist as suggested by the NMR data [37] to be discussed shortly, then an associated H–C–H correlation may also appear at higher r values and wholly (or partially) cancel any negative-going C–C–H feature.

Using the carbon–carbon second-shell peak centred at 2.5 Å, it has been possible to generate a carbon bond angle distribution which shows a principle peak centred on the tetrahedral angle, but extending towards 120°; precise statements cannot be made because the broad 2.5 Å peak has contributions from several carbon–carbon–carbon correlations.

This work may be compared with the results of Gaskell *et al* [38] in which they propose a 'new' form of carbon, intermediate between sp^2 and sp^3, to account for a slight inconsistency in first- and second-shell coordination numbers. However, their work assumes that all sp^2 carbon is in a graphitic environment; our results, although on rather different samples, would seem to suggest that this may be a poor approximation for low sp^2 concentrations. Their discrepancy between the first- and second-shell coordination numbers is reduced without the need to invoke this 'new' form of carbon if the sp^2 carbon is assumed to be all olefinic.

4.2. Inelastic neutron scattering

Inelastic neutron scattering (INS) is used here to examine in some detail the hydrogen bonding environments in a-C:H. The INS data were collected on the TFXA spectrometer, also at the ISIS spallation neutron source. In the incoherent approximation [39], the scattering function can be directly related to the vibrational density of states (VDOS) [39, 40]. In an amorphous system such as a-C:H there are many possible bonding environments, which give rise to vibrations over a range of frequencies. Due to its lighter mass, hydrogen vibrations are generally of higher frequency than those of the network, allowing a fully separate treatment. A further simplification is the univalence of hydrogen which restricts the number of local bonding environments that need to be considered to sp^3 CH, CH_2, and CH_3 groups, sp^2 olefinic and aromatic CH and olefinic CH_2 and sp^1 CH.

The experimental data can be modelled computationally [41] using a set of structural units representative of all the vibrational modes of each hydrogenated group (e.g. CH, CH_2) [42] and then refining the force constants associated with the model. In this way it is possible, in principle, to establish quantitatively the concentrations of each group that would be necessary to generate the observed VDOS.

The INS spectra for samples 1 and 2 are shown in figure 2. These can be split into two regions—a low-frequency region (<500 cm^{-1}) which is dominated by the scattering from residual quantities of the liquid nitrogen used to quench the samples and a high-frequency region (>500 cm^{-1}) consisting of localized CH_n stretch and bend vibrations. The CH_n bending vibrations lie between 700 and 1500 cm^{-1} and the CH_n stretch band and overtone of the CH_n stretching vibrations occur at 3000 and 2500 cm^{-1}, respectively.

Earlier NMR [43] and infrared (IR) spectroscopy [44] have suggested that hydrogen is predominantly bonded to sp^3 carbon so special consideration should be given to sp^3 CH_n groups. Further, IR spectroscopy by Vandentrop *et al* [45] has shown the sp^3 CH_3:CH_2 ratio in a-C:H to be very small, limiting the initial consideration to sp^3 CH and CH_2 groups.

From figure 2, the dominant peaks are at 875 and 1280 cm^{-1}, with additional component bands visible as shoulders either side of the 1280 cm^{-1} peak. Models based on the assignments of Dischler [44] failed to produce a good fit to the observed INS spectra [42]. In particular, the theoretical intensity at 700 cm^{-1} is too large and only a poor fit could be obtained to the 1280 cm^{-1} peak. However, if the CH and CH_2 bending vibrations are assigned in accordance with those of Dollish and co-workers [46], a good fit to the experimental data is obtained (see figure 2). The frequency assignments used are given in table 5. Modelling with sp^3 CH and CH_2 groups alone shows acceptable agreement with experiment: indeed any attempt to incorporate CH_3 groups at levels associated with more than ~10% of the hydrogen would produce a significant deterioration to the quality

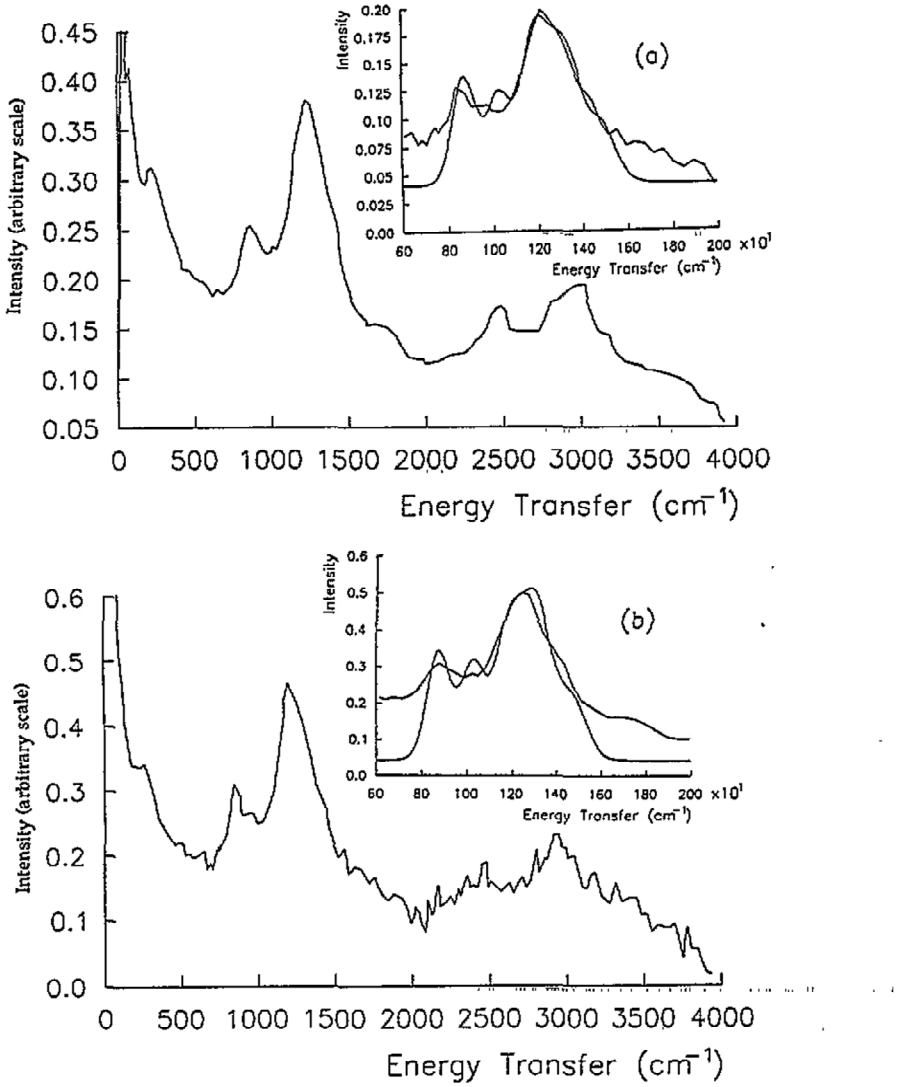

Figure 2. Inelastic neutron scattering spectra for sample 1 (a) and for sample 2 (b) obtained on the TFXA spectrometer [42]. Insets show the CLIMAX model fits to the experimental data.

of the fit.

The experimental results show that there are at least as many CH_2 groups as CH groups ($CH:CH_2 \sim 1$), contrary to what would be expected from a random distribution of hydrogen amongst carbon sites, and also from the analysis of the IR CH stretch vibration [44, 47] which suggested that CH sites would dominate. It should be noted, however, that the most recent IR studies [47], with a $CH:CH_2$ ratio of 1.5:1, actually imply more hydrogen in CH_2 groups than in CH groups and is therefore closer to our findings.

From the neutron diffraction results, the dominant carbon bonding environment is sp^2 hybridized even at the highest hydrogen content, of which olefinic carbon makes the dominant contribution. The C=C bond associated with an olefinic pair is resistant to rotation (unlike the C–C bond), thus adding extra rigidity. In a pure sp^2 carbon (e.g. graphite), this

Table 5. Frequency assignments used in modelling the INS spectra.

Vibration	Dischler [44]	Dollish *et al* [46]	This work
CC stretch	885 cm^{-1}	1132–885 cm^{-1}	875 cm^{-1}
CH_2 rock	700 cm^{-1}	1060–719 cm^{-1}	1030 cm^{-1}
CH bend	1370 cm^{-1}	1160 cm^{-1}	1190 cm^{-1}
CH_2 twist	1170 cm^{-1}	1310–1175 cm^{-1}	1300 cm^{-1}
CH_2 wag	1030 cm^{-1}	1411–1174 cm^{-1}	1330 cm^{-1}
CH_2 bend	1440 cm^{-1}	1473–1446 cm^{-1}	1470 cm^{-1}

would not normally result in a hard material, as the bonds are all in one plane, allowing delocalization of the π electrons throughout the interconnecting network; there are no interplanar bonds, resulting in a soft material. Tamor and Hass have, however, proposed a superhard three-dimensional sp^2 carbon [48], which may help our understanding of hard a-C:H.

In modelling the hardness of a-C:H, Robertson [49] agrees that olefinic carbon would contribute to network rigidity, but then ignores it on the grounds of very low concentration. Thus, by assuming that all sp^2 carbon is in aromatic or graphitic clusters, he obtains good agreement between his theoretical hardness calculations and experimental measurements for all but the lowest-sp^2-content films. Therefore this model must now be contrasted to the data presented here, where most carbon is sp^2 hybridized and yet there is both high olefinic content and hardness. The implication of this is that the olefinic carbon is responsible for the high hardness in these samples. The hydrogen would seem to be important more as an inhibitor of aromatic clustering than as a means of increasing the sp^3 'diamond-like' carbon as suggested by current models [2, 3, 50].

4.3. NMR

Various NMR techniques have been used to study the structural heterogeneity of samples 1 and 2 [37]. The standard CP/MAS (cross-polarization/magic angle spinning) experiments with and without dipolar dephasing yield quantitative information about the hybridization and the relative amount of hydrogenated and non-hydrogenated carbons. High-resolution combined rotation and multipulse spectroscopy (^{1}H–CRAMPS) experiments have been used to characterize the proton species whereas multiple-quantum NMR is a suitable tool to characterize the distribution of protons. For clustered distributions it is possible to determine the cluster size, i.e. the average number of interacting protons.

Figure 3 shows the ^{13}C CP spectrum as a function of the delay τ between the π pulse and the beginning of the ordinary CP experiment. The spectrum clearly shows sp^2 carbons at 130 ppm and a broad resonance due to sp^3 carbons at 65 ppm, similar to those obtained by other authors, [8] for example. By altering the recovery delay from 200 ms to 35 ms [37] the spectrum shown in figure 3 can be deconvoluted and the ratio of carbons with fast relaxing protons to those with slowly relaxing associated protons, sp^3:$sp^{3\prime}$, is determined as ~1:2. To determine the sp^2:sp^3 ratio, single-pulse ^{13}C experiments without CP but with TOSS (total suppression of sidebands) and decoupling were carried out [37]. This results in an estimated sp^2:sp^3 ratio of ~1.44, or 59±2%:41±2%, for both samples 1 and 2. Gated decoupling experiments can be used to determine the relative amount of hydrogenated and non-hydrogenated carbon atoms [37]. The results imply that only 20% of the sp^2 carbons are hydrogenated, whereas the corresponding relative amount is 35% for sp^3 carbons. If

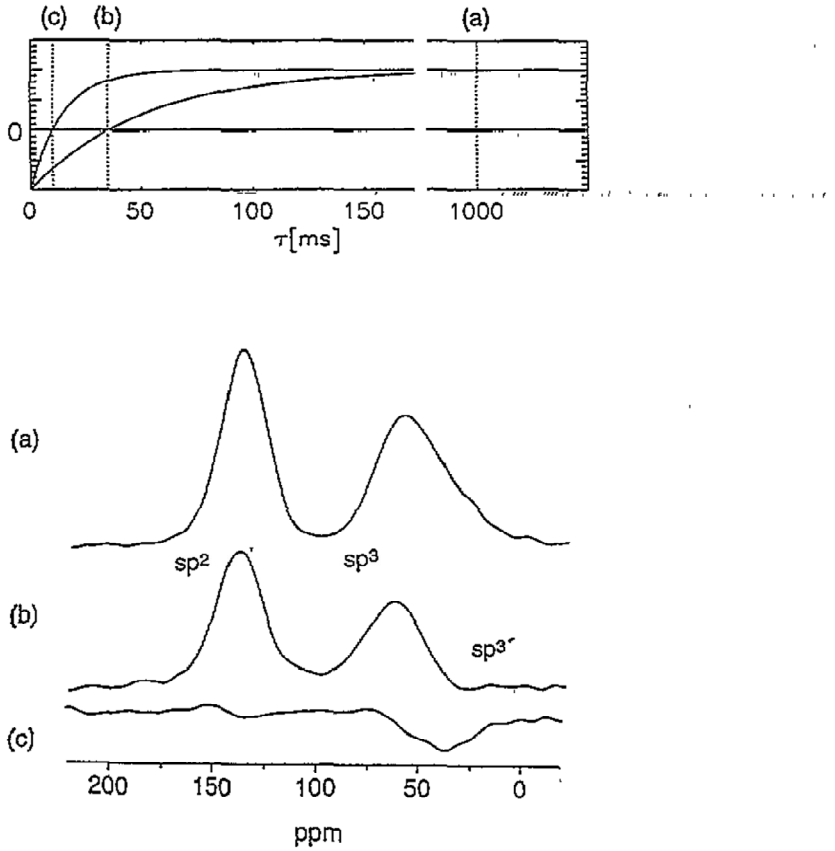

Figure 3. ^{13}C CP spectra as a function of the delay τ between the π pulse and the beginning of the ordinary CP experiment [37]. Case (a): normal spectrum showing sp^2 and sp^3 resonances as usual. Case (b): fast-relaxing protons were used for the cross-polarization. Case (c): slowly relaxing protons cross-polarize only $sp^{3'}$ carbons.

the slowly relaxing protons are assumed to form sp^3 CH_2 groups which form sections of polymer-like chains, and the fast relaxing protons are assumed to exist in sp^2 and sp^3 groups and these protons are statistically distributed, then a CH:CH_2 ratio of about 3:2 is obtained, with a corresponding ratio of 1:2 for sp^2 CH:sp^3 CH/CH_2 groups. This in turn results in a ratio of 1:3 for hydrogen atoms bound to sp^2 and sp^3 carbons respectively. Note that this is in broad agreement with the INS data which suggested that there were roughly equal amounts of CH and CH_2 groups.

In this analysis, two conclusions have been drawn: (1) the fast-relaxing protons are statistically distributed in the carbon network, and (2) other protons should be confined to small network regions. Using multiple quantum (MQ) NMR it is possible to look at these two different types of proton separately and to check the validity of these conclusions. MQ NMR [37] clearly shows the statistically distributed protons of the sp^2 and sp^3 CH groups, and gives a mean chain length of approximately five CH_2 units. Also, the breakdown of the ^1H spin diffusion, which would otherwise equilibrate the spin–lattice relaxation time, implies that these two hydrogenated environments are separated by regions of non-hydrogenated sp^2 carbons [37].

4.4. Computer simulation

Two different types of molecular dynamics simulation of a-C:H samples have been performed with parameters chosen to provide a close correspondence with the samples at the heart of the experimental study [24, 51]. The first of these [24] used the semiempirical density functional approach with 128 carbon atoms and 64 hydrogen atoms. Figure 4 shows the results as compared to the experimental neutron diffraction data. The total pair correlation functions presented in figure 4 agree very well with the experimental results and all the peaks and shoulders assigned in the analysis of the experimental data are found. Differences between the theoretical and experimental curves are mainly found for peaks related to correlations involving hydrogen atoms. This is particularly true for the H–H correlation at ~0.87 Å which is probably largely influenced by truncation effects in the Fourier transform and/or by the strong incoherent scattering of hydrogen in the neutron scattering experiment.

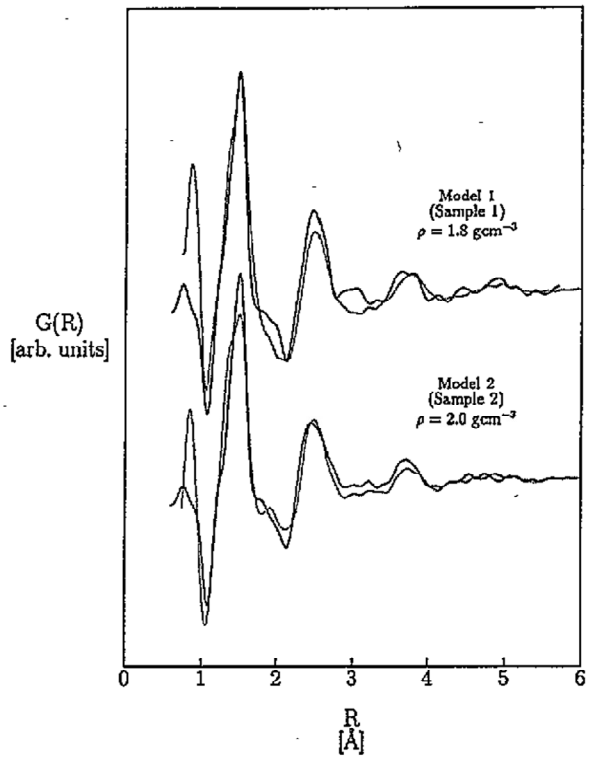

Figure 4. Total pair correlation function $G(r)$ for the molecular dynamics generated a-C:H models compared with the neutron diffraction data [24].

The models are mainly composed of twofold- and threefold-coordinated carbon atoms, with the fraction of fourfold coordinated sites not exceeding 30%. The models show a system of short chainlike segments with a markedly low tendency towards aromaticity. The sp^2 atoms are interconnected by homogeneously distributed sp^3 chainlike segments. Counting the different types of carbon bond gives a ratio between single and double bonds which agrees very well with the experimentally derived values. The models also confirm the existence of sp^3 H and sp^3 H_2 groups and can demonstrate the existence of H_2 molecules.

The number of rings with less than seven members is ~0.22 for both model structures, which is lower than in analogous simulations of diamond (2.0), graphite (0.5) and C_{60} (0.53). The major reason for this is the fact that the hydrogen atoms terminate network paths, which partly prevents carbon atoms from building closed loops in the network. Additionally, in the initial steps of the relaxation this is associated with a tendency to generate small chainlike segments as precursor clusters, which for atom numbers $\leqslant 5$ are more stable than corresponding ring clusters [52]. It is found that differently hybridized carbon atoms tend to cluster. Although π bonding is the main source for such cluster effects, the five-, six- and seven-membered rings are strongly cross-linked by the inclusion of at least one or two fourfold-coordinated atoms and are thus not aromatic. In one of the model structures one completely sp^2 bonded five-membered ring forming strong π bonds is found. However, this remains non-aromatic due to it being embedded into a strained bonding environment. Separated aromatic-like ring groups that are broadly discussed in the literature as responsible for the small electronic band gaps in these materials have not been formed under the constraint of a cross-linked rigid network even at the low mass densities considered in this simulation. The sp^2 atoms are rather arranged in olefinic groups (a conclusion which is also strongly supported by the analysis of coordination numbers).

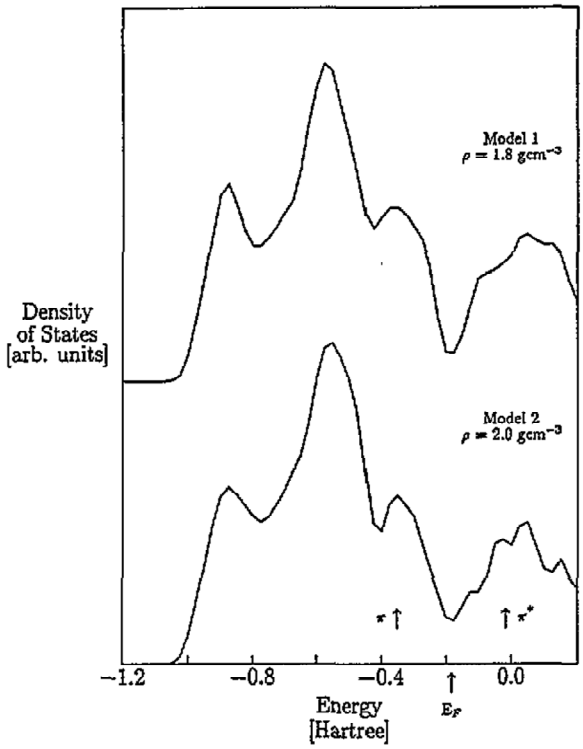

Figure 5. Electronic density of states for the two a-C:H models for molecular dynamics simulations [24].

Also, the total density of electronic states (TDOS) derived from the the simulation and shown in figure 5, indicates a gap width of ~1–2 eV for these models. The relatively small gaps obtained are not caused by the formation of separated more or less extended aromatic ring groupings in the a-C:H structures. They are, rather, a consequence of the

small π–π^* splitting realized by embedding the local π electron systems of π bonded atomic arrangements in the strained bonding environment of a rigid cross-linked network, in which 'mixed' bonds dominate. This is a very significant result given that previous structural models have been based on the results of theoretical modelling of the TDOS.

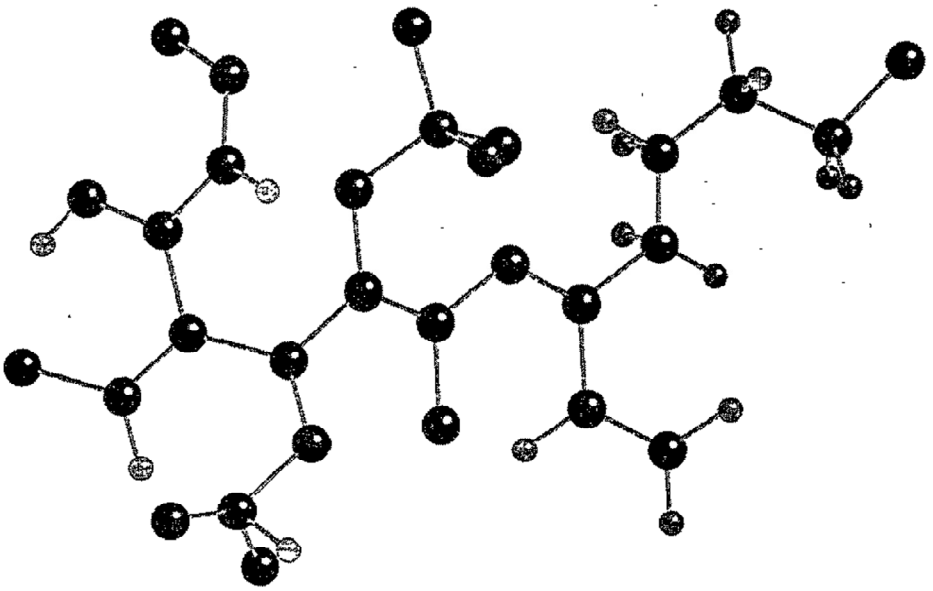

Figure 6. Schematic model of the microstructure of a-C:H based on the experimental data and showing heterogeneity in the structure on a nanometre scale.

From the results of similar work [52] it was suggested that the experimentally measured density may be significantly in error. However, the *ab initio* methods of [53] are not strongly dependent on this.

A second set of molecular dynamics results [51] using first-principles molecular dynamics again showed that the number of threefold-coordinated sites was higher than that of fourfold sites, and, although the agreement with the experimental data was not as good, also found no evidence for the existence of graphitic/aromatic units in the structure.

4.5. Summary

The experimental and molecular dynamics results can be summarized as follows

(1) The sp^2 C=C bond distance corresponds to olefinic rather than aromatic/graphitic bonding.

(2) The single:double bond ratio is evaluated as 2.5:1 from the neutron scattering results (up to a maximum of 3.7:1, given the curve fitting errors), but is estimated as ~4:1 from the NMR results.

(3) The numbers of CH and CH_2 groups are approximately equal: the number of CH_3 groups must be very small.

(4) The high hardness of this material can be explained in terms of olefinic carbon.

(5) The ratio for hydrogen atoms bound to sp^2 and sp^3 is 1:3, respectively.

(6) A mean chain length of approximately five CH_2 units is found.

(7) sp^2 and sp^3 CH groups are statistically distributed throughout the network.

(8) A small gap in the electronic density of states can be produced without the need to introduce graphitic/aromatic clusters into the structure.

(9) Models from molecular dynamics simulations fit the experimental data and show no aromatic/graphitic clusters.

The schematic 2D model presented in figure 6 illustrates how these conclusions may be incorporated into the structure of a-C:H.

5. Conclusions

Using the results obtained from three different experimental techniques and from MD simulations, it has been shown that current models for the structure of a-C:H, which rely on regions of clustered aromatic/graphitic sp^2 carbon, need revision. We have found no definitive experimental evidence for aromatic clustering in any published data, and certainly no results which could not be equally well explained in terms of olefinic sp^2 bonding. A new model is suggested which includes CH_2 chain segments, statistically distributed CH groups and regions of non-hydrogenated sp^3 and sp^2 carbon separating the regions of hydrogenated carbon. This model is consistent with all the experimental results. It has also been shown that the small band gap in a-C:H, and the electronic density of states which Robertson modelled using aromatic/graphitic clusters, can be reproduced by molecular dynamics simulations which do not include any such clusters.

References

[1] Elliott S R 1989 *Adv. Phys.* **38** 1
[2] Angus J C, Koidl P and Domitz S 1986 *Plasma Deposited Thin Films* ed J Mort and F Jansen (Boca Raton, FL: Chemical Rubber Company) ch 4, p 89
[3] Robertson J 1986 *Adv. Phys.* **35** 317
[4] Lettington A H 1991 *Diamond and Diamondlike Films and Coatings* ed J C Angus, R E Clausing, L L Horton and P Koidl (New York: Plenum)
[5] Aisenberg S and Kimock F M 1989 *Mater. Sci. Forum* **52 & 53** 1
[6] Lifshitz Y, Kasi S R and Rabalais J W 1989 *Mater. Sci. Forum* **52 & 53** 237
[7] Lifshitz Y, Kasi S R and Rabalais J W 1989 *Phys. Rev. Lett.* **62** 1290
[8] Jansen F, Machonkin M, Kaplan S and Hark S 1985 *J. Vac. Sci. Technol.* A **3** 605
[9] Dischler B, Sah R E and Koidl P 1983 *Plasma Chemistry—7th Int. Symp. (Eindhoven)* ed D C Schraum p 45
[10] Dischler B, Bubenzer A and Koidl P 1983 *Solid State Commun.* **48** 105
[11] Couderc P and Catherine Y 1987 *Thin Solid Films* **146** 93
[12] Tsai H 1989 *Mater. Sci. Forum* **52 & 53** 71
[13] Reimer J R, Vaughan R W, Knights J C and Lujan R A 1981 *J. Vac. Sci. Technol.* A **19** 53
[14] Polk D E 1971 *J. Non-Cryst. Solids* **5** 365
[15] Craig S and Harding G L 1982 *Thin Solid Films* **97** 345
[16] Smith F W 1984 *J. Appl. Phys.* **55** 764
[17] Miller D J and McKenzie D R 1983 *Thin Solid Films* **108** 257
[18] McKenzie D R, McPhedran R C, Savvides N and Botton L C 1983 *Phil. Mag.* B **48** 341
[19] McKenzie D R, Botten L C and McPhedran R C 1983 *Phys. Rev. Lett.* **51** 280
[20] Roberston J and O'Reilly E P 1987 *Phys. Rev.* B **35** 2946
[21] Robertson J 1991 *Prog. Solid State Chem.* **21** 199
[22] Bredas J L and Street G B 1985 *J. Phys. C: Solid State Phys.* **18** L651
[23] Frauenheim T, Blaudeck P, Stephan U and Jungnickel G 1993 *Solid State Commun.* **85** 997
[24] Jungnickel G, Frauenheim T, Blaudeck P and Stephan U and Newport R J 1994 *Phys. Rev.* B **50** 6709
[25] Fink J, Müller-Heinzerling T, Pflüger J, Scheerer B, Dischler B, Koidl P, Bubenzer A and Sah R E 1984 *Phys. Rev.* B **30** 4713
[26] Ramsteiner M and Wagner J 1987 *Appl. Phys. Lett.* **51** 1355

[27] Wesner D, Krummacher S, Carr R, Sham T K, Strongin M, Eberhardt W, Weng S L, Williams G, Howells M, Kampas F, Heald S and Smith F W 1983 *Phys. Rev.* B **28** 2152
[28] Oelhafen P and Ugolini D 1987 *Proc. EMRS* **17** 267
[29] Walters J K, Honeybone P J R, Huxley D W, Newport R J and Howells W S 1994 *Phys. Rev.* B **50** 831
[30] Kleber R, Jung K, Ehrhardt H, Mühling I, Breuer K, Metz H and Engelke F 1991 *Thin Solid Films* **205** 274
[31] 1992 *User Guide To Experimental Facilities At ISIS*
[32] Walters J K, Algar C D, Burke T M, Rigden J S, Newport R J, Bushnell-Wye G, Howells W S and Sattel S submitted
[33] Soper A K, Howells W S and Hannon A C 1989 *Rutherford Appleton Laboratory Report* RAL-89-046
[34] Newport R J 1988 *Neutron Scattering at a Pulsed Source* ed R J Newport, B D Rainford and R Cywinski (Bristol: Adam Hilger) ch 13, p 233
[35] Squires G L 1978 *Introduction to the Theory of Thermal Neutron Scattering* (Cambridge: Cambridge University Press)
[36] Gunn J M F 1988 *Neutron Scattering at a Pulsed Source* ed R J Newport, B D Rainford and R Cywinski (Bristol: Adam Hilger) ch 1, p 5
[37] Jäger C, Gottwald J, Spieß H W and Newport R J 1994 *Phys. Rev.* B **50** 846
[38] Gaskell P H, Saeed A, Chieux P and McKenzie D R 1992 *Phil. Mag.* B **66** 155
[39] Axe J D 1976 *Physics of Structurally Disordered Materials* ed S S Mitra (New York: Plenum) p 507
[40] Tomkinson J 1988 *Neutron Scattering at a Pulsed Source* R J Newport, B D Rainford and R Cywinski (Bristol: Adam Hilger) ch 18, p 324
[41] Kearley G J and Tomkinson J 1990 *Inst. Phys. Conf. Ser. 107* (Bristol: Insitute of Physics) p 245
[42] Honeybone P J R, Newport R J, Walters J K, Howells W S and Tomkinson J 1994 *Phys. Rev.* B **50** 839
[43] Petrich M A 1989 *Mater. Sci. Forum* **52** 377
[44] Dischler B 1987 *Amorphous Hydrogenated Carbon Films* ed P Koidl and P Oelhafen (Les Ulis: Editions de Physiques) p 189
[45] Vandentrop G J, Kawasaki M, Kobayashi K and Somorjai G A 1991 *J. Vac. Sci. Technol.* A **9** 1157
[46] Dollish F R, Fately W G and Bentley F F 1974b *Characteristic Raman Frequencies* (New York: Wiley)
[47] Koidl P, Wild Ch, Dishler B, Wagner J and Ramsteiner M 1989 *Mater. Sci. Forum* **52 & 53** 41
[48] Tamor M A and Hass K C 1990 *J. Mater. Res.* **5** 2273
[49] Robertson J 1992 *Phys. Rev. Lett.* **68** 220
[50] Robertson J 1991 *Diamond and Diamondlike Films and Coatings* ed J C Angus, R E Clausing, L L Horton and P Koidl (New York: Plenum) p 331
[51] Iarlori S, Galli G and Martini O 1994 *Phys. Rev.* B **49** 7060
[52] Blaudeck P, Frauenheim Th, Seifert G and Fromm E 1992 *J. Phys.: Condens. Matter* **4** 6389
[53] Drabold D A, Fedders P A and Strumm P 1994 *Phys. Rev.* B **49** 16 415